Hybridized Frequency Combs in Multimode Cavity Electromechanical System

Sishi Wu[,1] Yulong Liu[,2,*] Qichun Liu[,2] Shuai-Peng Wang[,1] Zhen Chen[,2] and Tiefu Li[3,2,†]

[1]*Quantum Physics and Quantum Information Division, Beijing Computational Science Research Center, Beijing 100193, China*
[2]*Beijing Academy of Quantum Information Sciences, Beijing 100193, China*
[3]*School of Integrated Circuits and Frontier Science Center for Quantum Information, Tsinghua University, Beijing 100084, China*

The cavity electromechanical devices with radiation-pressure interaction induced Kerr-like nonlinearity are promising candidates to generate microwave frequency combs. We construct a silicon-nitride membrane based superconducting cavity electromechanical device and study two mechanical modes synergistic frequency combs. Around the threshold of intracavity field instability, we first show independent frequency combs with tooth spacing equal to each mechanical mode frequency. At the overlap boundaries of these two individual mechanical mode mediated instability thresholds, we observe hybridization of frequency combs based on the cavity field mediated indirect coupling between these two mechanical modes. The spectrum lines turn out to be unequally spaced, but can be recognized in combinations of the coexisting frequency combs. Beyond the boundary, the comb reverts to the single mode case, and which mechanical mode frequency will the tooth spacing be depends on the mode competition. Our work demonstrates mechanical mode competition enabled switchability of frequency comb tooth spacing and can be extended to other devices with multiple nonlinearities.

Frequency combs are spectra of phase-coherent evenly spaced narrow lines and were initially invented in laser for frequency metrology [1,2]. Originally, the optical frequency combs were developed in the 1990s as rulers to measure large optical frequency differences and to provide a direct link between optical and microwave frequency [3,4]. After two decades of development, apart from the application in metrology, the frequency combs have become a powerful tool in molecular fingerprinting [5], atomic clocks [6], attosecond science [7], optical communications [8–10], etc. Toward further application on quantum information and quantum computation, intrinsic phase matching of frequency combs makes it a promising platform for realizing multipartite entanglement and cluster states, which are building blocks in continuous variable quantum computation [11–15].

In addition to atomic-gas-based optical frequency combs, microcavities with Kerr nonlinearity [16–18] have also attracted intense attention. To explore the microwave frequency combs, electromechanical devices can be a suitable platform. They have relative strong single-photon couplings [19–22] and can work at millikelvin temperature, which makes them well isolated from most thermal noise environments. Meanwhile, sideband cooling technology [23–25] enables electromechanical devices to work in the quantum regime. Additionally, the capability of its integration with microwave superconducting circuits makes it a considerable composite for hybrid quantum computing systems [26]. Here, we report on the observation of microwave frequency combs in a multimode electromechanical system composed of a three-dimensional (3D) aluminum (Al) superconducting cavity and a metalized silicon nitride (SiN) membrane.

Besides each single mechanical mode mediated frequency comb with repetition rate of the respective characteristic frequency, we observe finer spectra, but with unequally spaced distribution. Such spectra result from hybridization of single mechanical mode mediated frequency combs, and occur only at the overlap boundary of pump conditions for two individual mechanical induced cavity field instability thresholds. Thus, in our experiment, the pump frequency and power can be used to *in situ* switch the frequency combs with different tooth spacing.

Multimode cavity electromechanical device.—As is presented in Fig. 1(a), the sample is composed of a SiN membrane based mechanical compliant capacitor and a 3D aluminium cavity. The SiN membrane holds multiple mechanical modes with different mode shape. Here, we consider the lowest two mechanical modes with membrane center drumhead vibration frequencies of Ω_{m1} and Ω_{m2}, respectively. The internal chamber of the rectangle Al block supports the cavity mode, with a resonance frequency of Ω_c. Figure 1(b) gives detailed information of the mechanically compliant capacitor chip. Two large Al coupling capacitors (gray parts on the bottom chip) lying on the high-resistance silicon substrate (blue) ensure maximum single-photon coupling strength while introducing the minimum stress disturbance for SiN membrane [27,28]. High-stress SiN films (brown parts on the flip chip) are evaporated, with a 20 nm Al electrode on its back (gray).
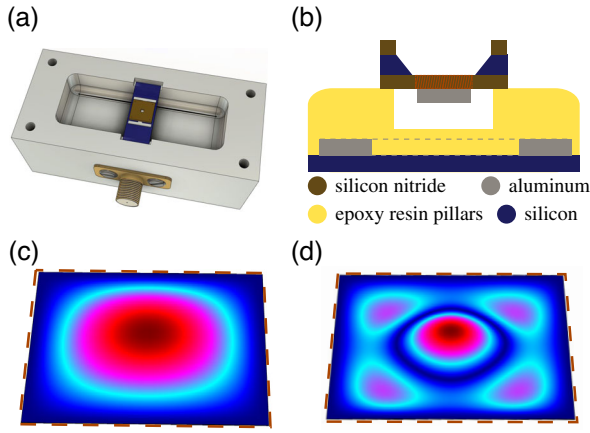
FIG. 1.   (a) Illustration of sample encapsulation. The mechanically compliant capacitor chip is placed at the center of the rectangular Al box. (b) Side view of the mechanically compliant capacitor chip. The color indicates different materials. (c),(d) Simulated motion of the first and the second mechanical modes (with a drumhead vibration at the membrane center) of the mechanical oscillating element, respectively.

The reddish brown shaded area represents the suspended SiN membrane, supporting the mechanical oscillating part. The mechanical modes are simulated via the finite element method, leading to expected eigenmode frequencies of 755 kHz and 1.755 MHz, as shown in Figs. 1(d) and 1(e), respectively.

Our experiment is carried out in a dilution refrigerator [29]. The pump signal (Ω_d) is injected into the cavity through a circulator. Before reaching the sample, the input signal is attenuated to reduce background noise. The reflected signal (Ω_s) is split into two, one of which is read by a network analyzer and the other is used to do the spectrum analysis. To avoid amplifier saturation, the reflected pump signal is well canceled by using a directional coupler [29].

Working in a frame rotating at the frequency of the pump tone, the Hamiltonian of such a multimechanical mode electromechanical system can be expressed as [36–41]

$$H_{\text{syst}}/\hbar = \left(-\Delta_{dc} - i\frac{\kappa}{2}\right)a^\dagger a + \sum_{j=1,2}\left(\Omega_{mj} - i\frac{\gamma_j}{2}\right)b_j^\dagger b_j$$
$$+ \sum_{j=1,2} g_j a^\dagger a(b_j + b_j^\dagger) + i\sqrt{\kappa_e}S_{\text{in}}(a^\dagger - a), \quad (1)$$

where $\Delta_{dc} = \Omega_d - \Omega_c$, and the label j in Ω_{mj} indicates the order of the mechanical mode referred. Coefficient g_j represents the single-photon coupling strength between the cavity and the jth mechanical mode, respectively. The coupling efficiency between the sub-miniature A (SMA) connector and the cavity is labeled as κ_e. S_{in} describes the amplitude of the pump signal normalized to a photon flux at the input of the cavity, and is defined as $S_{\text{in}} = \sqrt{P_d/\hbar\Omega_d}$, where P_d (in the unit of watt) is the pump power at the input of the cavity. Additionally, a ($a^\dagger$) and b_j ($b_j^\dagger$) represent annihilation (creation) operators for cavity and the jth mechanical mode, respectively.

According to precharacterization by measuring the mechanical spectra [29], frequencies of the mechanical oscillator are $\Omega_{m1}/2\pi = 756$ kHz for the first mode (mode 1), with damping rate $\gamma_1/2\pi = 2.32$ Hz, and $\Omega_{m2}/2\pi = 1.750$ MHz for the second mode (mode 2), with damping rate $\gamma_2/2\pi = 0.30$ Hz. The 3D cavity is characterized to have frequency of $\Omega_c/2\pi = 5.31$ GHz and damping rate of $\kappa/2\pi = 380$ kHz, which implies that the electromechanical system is within the resolved-sideband regime ($\Omega_{mj} > \kappa$) [36–43]. The single-photon coupling strengths $g_1/2\pi = 0.49$ Hz and $g_2/2\pi = 0.07$ Hz are calibrated from the measurements based on a frequency modulation technique [29].

As implied by the system Hamiltonian, interaction of cavity and membrane results in photon number dependent cavity frequency shift, which in turn changes reflection. The equations of motion are

$$\dot{a} = \left\{i\left[\Delta_{dc} - \sum_{j=1,2}g_j(b_j + b_j^\dagger)\right] - \frac{\kappa}{2}\right\}a + \sqrt{\kappa_e}S_{\text{in}}, \quad (2a)$$

$$\dot{b}_j = -\left(i\Omega_{mj} + \frac{\gamma_j}{2}\right)b_j - ig_j a^\dagger a. \quad (2b)$$

Similar to the frequency comb induced by the Kerr oscillator [44–46], such electromechanical couplings can also result in a frequency comb for pump condition beyond threshold of intracavity field instability [37], whereas the cavity field can be expressed as a weighted sum of series Bessel functions [29,38].

Formation and evolution of electromechanical frequency combs.—First, we explore the formation of frequency combs under the exact blue sideband pump. The detuning between pump frequency to the cavity frequency matches one of the mechanical mode frequencies. Therefore, the cavity nonlinearity will be mainly determined accordingly by one mechanical motion. We then conduct the heterodyne detection [29] of the reflected spectrum, whose x axis is labeled as Ω_s. When $\Delta_{dc} = \Omega_{m1}$, as shown in Fig. 2(a), only one peak at $\Omega_s = \Omega_d$ is observed initially.

When the pump power increases above -75 dBm, the frequency comb occurs with the tooth spacing equaling Ω_{m1}, and the comb bandwidth grows steadily with higher drive power. The typical electromechanical frequency comb mediated by mechanical mode 1 is shown in Fig. 2(b), with a fixed pump power at -29 dBm, as an example. Further increasing the pump power, higher-order nonlinearity participates and results in abruptly broadened dense spectra. Analogously, when the driving is blue detuned close to the frequency of mechanical mode 2, i.e., $\Delta_{dc} = \Omega_{m2}$, the spectral evolution versus drive power
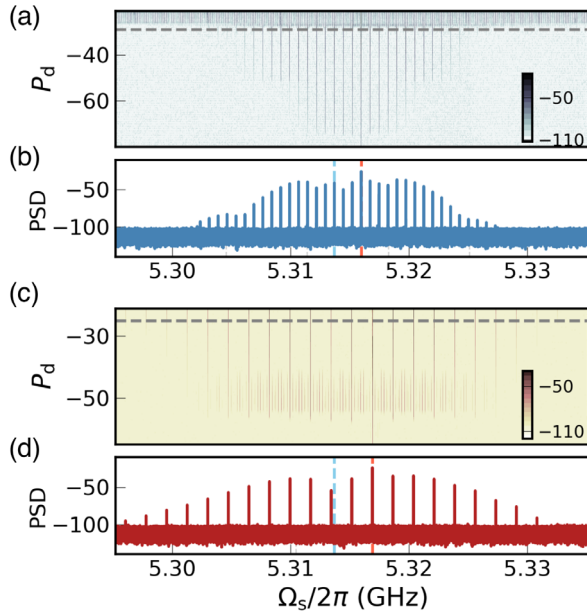
FIG. 2. Single mechanical mode mediated frequency combs. (a),(c) Detected comb evolution along increased pump power with detuning of $\Delta_{dc} \approx \Omega_{mj}$. (b),(d) An example of comb spectrum, and is marked as gray dashed line in (a) and (c) respectively. The pump power P_d is in the unit of dBm. Unit of the power spectral density (PSD) is dBm/Hz. The pump frequency is marked as vertical red dashed line, and cavity frequency is marked as vertical blue dashed line.
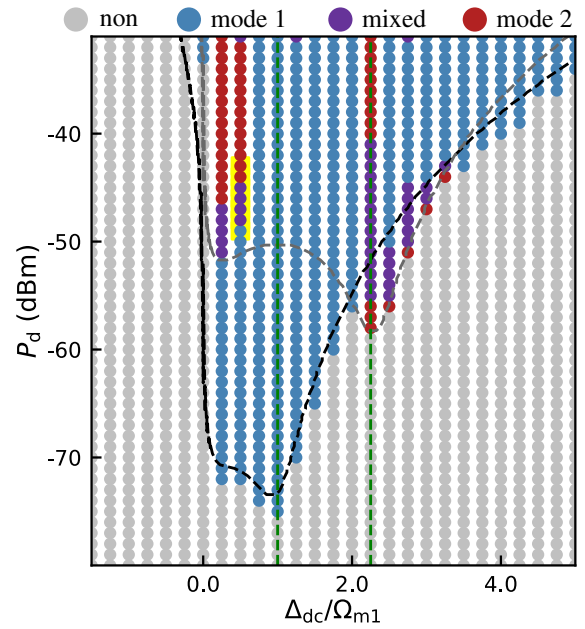
FIG. 3. Formation and evolution of frequency combs. Spectral responses are sorted into four types, and are marked in different colors as dots. Black (gray) dashed line is single first (second) mechanical mode induced cavity field instability threshold. Two green dashed lines refer to pump condition chosen for Fig. 2, and yellow highlighted region is the chosen for further analysis in Fig. 4.

is exhibited in Fig. 2(c). Under a driving power given at -25 dBm, the electromechanical frequency comb mediated by mechanical mode 2 is shown in Fig. 2(d), with the tooth spacing equaling Ω_{m2}. Extra spectral lines in Fig. 2(c) are caused by the nonideal pump frequency, which is strictly required due to the comparatively small g_2 and γ_2. The more accurate Δ_{dc} is to Ω_{m2}, the clearer the spectra would be. Similar to that in the micromechanical resonator case [47], symmetry of frequency combs about the pump frequency (location marked as red dashed line) is influenced by cavity transmission (frequency location marked as blue dashed line).

We further study dependency of the spectrum evolution on pump frequency. As shown in Fig. 3, frequency spectra with a single peak at Ω_d are detected initially, which are marked as gray dots. Along increased pump power, the cavity field becomes unstable, and frequency combs are formed. Primary instability occurs around $\Delta_{dc} = \Omega_{m1}$, where the first mechanical mode influenced cavity field is most efficiently pumped. Subsequently, mode-1 mediated frequency combs are formed (blue dots in Fig. 3), and the frequency combs are similar to the spectra presented in Fig. 2(b). Similarly, mode-2 influenced cavity field instability occurs initially at $\Delta_{dc} = \Omega_{m2}$. Thereafter, second mechanical mode mediated frequency combs are formed (marked by red dots in Fig. 3), and the frequency combs are similar to the spectra presented in Fig. 2(d).

The measured threshold of the pump condition (including the driving power and frequency) to form frequency combs is shown in Fig. 3. The boundary can be fitted as a combination of the black and gray dashed lines. The black dashed line is the theoretically analyzed instability threshold of the cavity field caused by the electromechanical coupling with mode 1. Meanwhile, the gray dashed line marks the threshold of frequency comb generation mediated by mode 2 [29]. The overlap boundary for these two single mechanical mode induced instability thresholds enables transition between mode-1 mediated frequency combs and mode-2 mediated frequency combs, where hybridized spectra emerge (purple dots in Fig. 3). The teeth of the complex spectrum are unequally spaced, but can be identified as a set of coexisting frequency combs. Such hybridization results from effective coupling between two individual mechanical modes via the cavity field [36]. It is worth noting that for the most pump conditions, due to mode competition, one mechanical mode small-amplitude gain tends to suppress another [29].

Frequency Combs hybridization.—To study detailed features of frequency combs hybridization, we focus on the comb evolution when the pump detuning is fixed at $\Delta_{dc}/\Omega_{m1} = 0.5$, and pump power varies from -49 to -43 dBm (as shown in Fig. 4, corresponding to the yellow region in Fig. 3). Under this condition, evolution of frequency combs is transformed from the mode-1
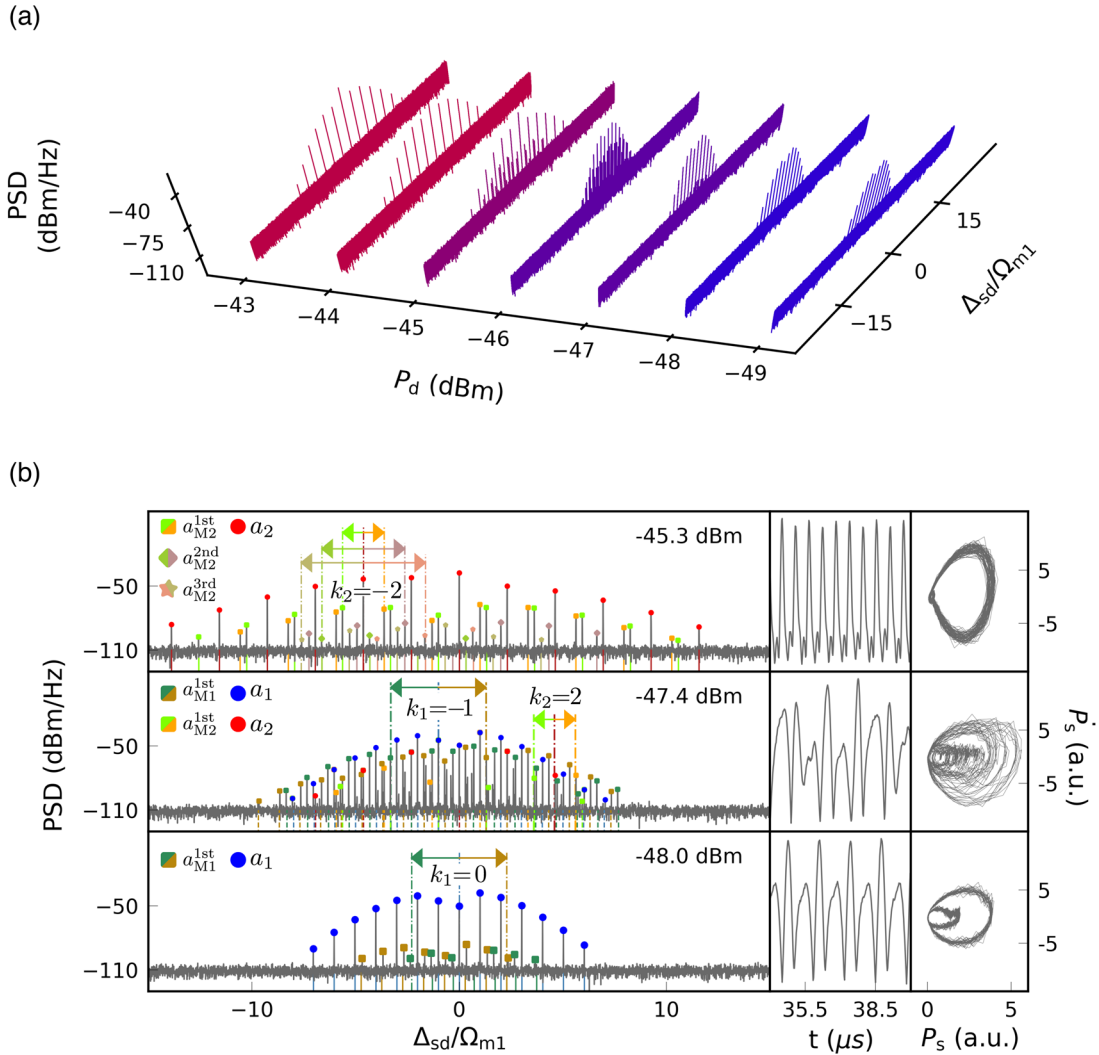
FIG. 4. Transitional behaviors of frequency combs. (a) Pump power dependent spectrum evolution from first mechanical mode mediated frequency combs (blue) toward second mechanical mode mediated frequency combs (red), where $\Delta_{sd} = \Omega_s - \omega_d$. Hybridized frequency combs (purple) emerge during the transition. (b) The left-hand column exhibits the spectra within frequency domain, whose pump powers are annotated. Experimental data are plotted in gray. Configurable teeth are marked in colored dots. As labeled, blue (red) round dots refer to teeth spaced in the first (second) mechanical mode frequency, i.e., $a_1(t)$ [$a_2(t)$] terms described in the text. Green and yellow square dots refer to mixed sidebands of the second order, i.e., $a_{Mj}^{1st}(t)$, where $M = s, d$ and $j = 1, 2$. Similarly, diamond dots refer to $a_{Mj}^{2nd}(t)$, and star dots refer to $a_{Mj}^{3rd}(t)$. Examples of mixing procedures are picked and expressed in paired arrows, centered on single mechanical mode based tooth with order of k_j. The middle column of (b) exhibits the accordingly behavior in time domain. The right-hand column exhibits the accordingly optical trajectories in phase space, with label P_s representing intracavity field power in an arbitrary unit (a. u.).

determined type to the mode-2 determined type. Initially, the spectra can be expressed as $a_1(t) = \sum_{k_1=-\infty}^{\infty} \alpha_{k_1} \exp(\Omega_d t) \exp(-ik_1\Omega_{m1}t)$. The integer label k_1 represents the order of the comb teeth, with amplitude of α_{k_1}, and detuning of $k_1\Omega_{m1}$ (from the pump frequency). Note that, due to dependency of α_{k_1} on the cavity field distribution, symmetry of the comb envelope about Ω_d can be broken, especially for large Δ_{dc}. As the pump power increased, the second mechanical mode participates and leads to sideband mixing, resulting in hybridized frequency combs, which can be expressed as

$$a(t) = a_1(t) + a_2(t) + a_s(t) + a_d(t), \quad (3)$$

where $a_2(t)$ represents teeth detuned from the center by $k_2\Omega_{m2}$, and can be written as $a_2(t) = \sum_{k_2=-\infty}^{\infty} \alpha_{k_2} \exp(\Omega_d t) \exp(-ik_2\Omega_{m2}t)$. Similarly, teeth detuned by the sum and difference of several mechanical mode frequencies are

$$a_s(t) = \sum_{k_{s1},k_{s2}=-\infty}^{\infty} \alpha_{k_s} \exp(\Omega_d t) \exp[-i(k_{s1}\Omega_{m1} + k_{s2}\Omega_{m2})t],$$

$$a_d(t) = \sum_{k_{d1},k_{d2}=-\infty}^{\infty} \alpha_{k_d} \exp(\Omega_d t) \exp[i(k_{d1}\Omega_{m1} - k_{d2}\Omega_{m2})t].$$

When we further increase the pump power, mechanical oscillation is fully excited onto the higher mode, and thus $a(t) = a_2(t)$.

Specifically, degeneracy of k_j, k_{sj}, and k_{dj} can be concluded as the order of mixing. For an example, when the pump condition is set to be $\Delta_{dc} = 0.5\Omega_{m1}$ and $P_d = -48.0$ dBm [see the lower left-hand panel of Fig. 4(b)], the spectrum can be expressed as $a(t) = a_1(t) + a_{s1}^{1st}(t) + a_{d1}^{1st}(t)$, with $a_{M1}^{1st} = \sum_{k_1} \alpha_{M_1}^{1st} \exp(\Omega_d t) \exp[i(k_1\Omega_{m1} \pm \Omega_{m2})t]$ for $M = s, d$, which represents teeth of the same spacing with $a_1(t)$ but detuned by $\pm\Omega_{m2}$. This is a mode-1 dominated frequency comb dressed by mode 2. Phenomenally, the spectrum contains mainly teeth spaced in first mechanical mode frequency and first-order mixed sidebands centered by the k_1th teeth. Subsequently, higher-order mixed sidebands occur, of which the -45.3 dBm pumped case can be an example. This is a second mechanical mode dominated frequency comb, dressed by the first mechanical mode.

As shown in the upper left-hand panel of Fig. 4(b), for the additional frequency comb mediated from the first-order mixing procedure (marked as the shortest orange and green arrows), teeth (marked as square dots) are spaced in Ω_{m2} and detuned by $\pm\Omega_{m1}$ from $a_2(t)$, with k_2 as the relative order. Further, higher order with teeth detuned by $\pm2\Omega_{m1}$ (marked as diamond dots) and $\pm3\Omega_{m1}$ (marked as star dots) calls for consideration. All sum-frequency components are paired with difference terms of the same k_2 distribution. The total spectrum of this case can then be expressed as $a(t) = a_2(t) + \sum_{M=s,d}[a_{M2}^{1st}(t) + a_{M2}^{2nd}(t) + a_{M2}^{3rd}(t)]$. During transformation of the two single mechanical mode dominated frequency comb regimes, there exist more complicated mixing procedures, e.g., with -47.4 dBm pumped [see the center left-hand panel of Fig. 4(b)], which provides finer spectrum structure. Additionally, around $\Delta_{dc}/\Omega_{m2} = 1$, similar transitional behavior (from the mode-2 based to the mode-1 based frequency combs) occurs.

Conclusion.—In this Letter, we have constructed a SiN membrane based multimode superconducting cavity electromechanical device. Under cryogenic temperature, we experimentally demonstrate the evolution of frequency spectra dominated by the electromechanical nonlinearity. The threshold of cavity field instability corresponds to the formations of frequency combs. Furthermore, the frequency comb hybridization locates in two overlapped unstable boundaries, i.e., where the pump detuning is near half of the frequency of mode 1, or around the frequency of mode 2. Formation for single mechanical mode mediated frequency combs and evolution toward hybridized frequency combs are both demonstrated. Specifically, teeth positions of hybridized frequency combs are analyzed. At the early or late stage of the transitions, the comb teeth are spaced in frequency of one mechanical mode, and are accompanied by additional mixed sidebands with detuning of integer multiple of another.

This work could help us to understand the coexistence and hybridization of frequency combs which yields more refined frequency combs spectroscopy. Such spectroscopy exhibits mixed sidebands, accompanied by sister sidebands. As a foresight, the mode competition and hybridization provide an alternative method, besides traditional spontaneous and stimulated parametric conversion, to construct multimode entangled photon states, which provides diverse application on quantum source and quantum information processing. One prerequisite for the electromechanical microcombs entering the quantum regime is the preparation of the mechanical modes into their ground states. Introducing amplitude-modulated cooling tone, the mechanical modes with asymptotic orbits could be cooled down to their ground state when the frequency comb occurs.

---

*liuyl@baqis.ac.cn

†litf@tsinghua.edu.cn

[1] T. Fortier and E. Baumann, Commun. Phys. **2**, 153 (2019).

[2] F. Karim, S. K. Scholten, C. Perrella, and A. N. Luiten, Phys. Rev. Applied **14**, 024087 (2020).

[3] M. Kourogi, K. Nakagawa, and M. Ohtsu, IEEE J. Quantum Electron. **29**, 2693 (1993).

[4] S. A. Diddams, D. J. Jones, J. Ye, S. T. Cundiff, J. L. Hall, J. K. Ranka, R. S. Windeler, R. Holzwarth, T. Udem, and T. W. Hänsch, Phys. Rev. Lett. **84**, 5102 (2000).

[5] S. A. Diddams, L. Hollberg, and V. Mbele, Nature (London) **445**, 627 (2007).

[6] C. Gohle, T. Udem, M. Herrmann, J. Rauschenberger, R. Holzwarth, H. A. Schuessler, F. Krausz, and T. W. Hänsch, Nature (London) **436**, 234 (2005).

[7] P. Tzallas, D. Charalambidis, N. Papadogiannis, K. Witte, and G. D. Tsakiris, Nature (London) **426**, 267 (2003).

[8] V. Torres-Company and A. M. Weiner, Laser Photonics Rev. **8**, 368 (2014).

[9] A. Choudhary, M. Pelusi, D. Marpaung, T. Inoue, K. Vu, P. Ma, D.-Y. Choi, S. Madden, S. Namiki, and B. J. Eggleton, Opt. Lett. **42**, 5074 (2017).

[10] A. L. Gaeta, M. Lipson, and T. J. Kippenberg, Nat. Photonics **13**, 158 (2019).

[11] J. Roslund, R. M. De Araujo, S. Jiang, C. Fabre, and N. Treps, Nat. Photonics **8**, 109 (2014).

[12] M. Chen, N. C. Menicucci, and O. Pfister, Phys. Rev. Lett. **112**, 120505 (2014).

[13] M. Tian and D. Vega, Phys. Rev. A **100**, 042328 (2019).

[14] O. Pfister, J. Phys. B **53**, 012001 (2020).

[15] Y. Cai, Y. Xiang, Y. Liu, Q. He, and N. Treps, Phys. Rev. Research **2**, 032046(R) (2020).

[16] T. J. Kippenberg, R. Holzwarth, and S. A. Diddams, Science **332**, 555 (2011).

[17] S. Fujii, A. Hori, T. Kato, R. Suzuki, Y. Okabe, W. Yoshiki, A.-C. Jinnai, and T. Tanabe, Opt. Express **25**, 28969 (2017).

[18] C. Xu, J. Ma, C. Ke, Z. Zeng, L. Shen, W. Weng, Y. Zhang, and Y. Huang, Appl. Phys. Lett. **114**, 091104 (2019).

[19] J. D. Teufel, D. Li, M. Allman, K. Cicak, A. Sirois, J. Whittaker, and R. Simmonds, Nature (London) **471**, 204 (2011).

[20] J.-M. Pirkkalainen, S. Cho, J. Li, G. Paraoanu, P. Hakonen, and M. Sillanpää, Nature (London) **494**, 211 (2013).

[21] T. T. Heikkilä, F. Massel, J. Tuorila, R. Khan, and M. A. Sillanpää, Phys. Rev. Lett. **112**, 203603 (2014).

[22] J.-M. Pirkkalainen, E. Damskägg, M. Brandt, F. Massel, and M. A. Sillanpää, Phys. Rev. Lett. **115**, 243601 (2015).

[23] L. Yong-Chun, H. Yu-Wen, W. C. Wei, and X. Yun-Feng, Chin. Phys. B **22**, 114213 (2013).

[24] J.-H. Gan, Y.-C. Liu, C. Lu, X. Wang, M. K. Tey, and L. You, Laser Photonics Rev. **13**, 1900120 (2019).

[25] D.-G. Lai, J.-F. Huang, X.-L. Yin, B.-P. Hou, W. Li, D. Vitali, F. Nori, and J.-Q. Liao, Phys. Rev. A **102**, 011502(R) (2020).

[26] A. Clerk, K. Lehnert, P. Bertet, J. Petta, and Y. Nakamura, Nat. Phys. **16**, 257 (2020).

[27] Y. Liu, J. Mummery, J. Zhou, and M. A. Sillanpää, Phys. Rev. Applied **15**, 034004 (2021).

[28] Y. Liu, Q. Liu, S. Wang, Z. Chen, M. A. Sillanpää, and T. Li, Phys. Rev. Lett. **127**, 273603 (2021).

[29] See Supplemental Material at http://link.aps.org/supplemental/10.1103/PhysRevLett.128.153901 for details about experimental setup, single-photon coupling strength, threshold of stability, effective phonon-phonon coupling, and multimechanical mode competition, which includes Refs. [30–38].

[30] S. E. Nigg, H. Paik, B. Vlastakis, G. Kirchmair, S. Shankar, L. Frunzio, M. H. Devoret, R. J. Schoelkopf, and S. M. Girvin, Phys. Rev. Lett. **108**, 240502 (2012).

[31] M. Gorodetksy, A. Schliesser, G. Anetsberger, S. Deleglise, and T. J. Kippenberg, Opt. Express **18**, 23236 (2010).

[32] X. Zhou, F. Hocke, A. Schliesser, A. Marx, H. Huebl, R. Gross, and T. J. Kippenberg, Nat. Phys. **9**, 179 (2013).

[33] F. Marquardt, J. G. E. Harris, and S. M. Girvin, Phys. Rev. Lett. **96**, 103901 (2006).

[34] L. Mercadé, K. Pelka, R. Burgwal, A. Xuereb, A. Martínez, and E. Verhagen, Phys. Rev. Lett. **127**, 073601 (2021).

[35] Y. Hu, S. Ding, Y. Qin, J. Gu, W. Wan, M. Xiao, and X. Jiang, Phys. Rev. Lett. **127**, 134301 (2021).

[36] L. F. Buchmann and D. M. Stamper-Kurn, Phys. Rev. A **92**, 013851 (2015).

[37] M.-A. Miri, G. D' Aguanno, and A. Alù, New J. Phys. **20**, 043013 (2018).

[38] U. Kemiktarak, M. Durand, M. Metcalfe, and J. Lawall, Phys. Rev. Lett. **113**, 030802 (2014).

[39] M. Aspelmeyer, T. J. Kippenberg, and F. Marquardt, Rev. Mod. Phys. **86**, 1391 (2014).

[40] C. Jiang, Y.-L. Liu, and M. A. Sillanpää, Phys. Rev. A **104**, 013502 (2021).

[41] C. F. Ockeloen-Korppi, M. F. Gely, E. Damskägg, M. Jenkins, G. A. Steele, and M. A. Sillanpää, Phys. Rev. A **99**, 023826 (2019).

[42] A. Schliesser, R. Rivière, G. Anetsberger, O. Arcizet, and T. J. Kippenberg, Nat. Phys. **4**, 415 (2008).

[43] Y.-L. Liu, C. Wang, J. Zhang, and Y.-x. Liu, Chin. Phys. B **27**, 024204 (2018).

[44] Z. R. Gong, H. Ian, Y.-x. Liu, C. P. Sun, and F. Nori, Phys. Rev. A **80**, 065801 (2009).

[45] S. Aldana, C. Bruder, and A. Nunnenkamp, Phys. Rev. A **88**, 043826 (2013).

[46] Y.-L. Liu, R. Wu, J. Zhang, Ş. K. Özdemir, L. Yang, F. Nori, and Y.-x. Liu, Phys. Rev. A **95**, 013843 (2017).

[47] Q. Yang, X. Wang, R. Huan, L. Xu, Y. Xu, Z. Jiang, and X. Wei, Appl. Phys. Lett. **118**, 223502 (2021).